

2

AD-A224 801

DTIC FILE COPY

OFFICE OF NAVAL RESEARCH  
Contract N00014-87-J-1118  
R & T Code 4133016  
Technical Report No. 16

**An Examination of the Relationship Between Surface Enhanced Raman Scattering (SERS)  
Intensities and Surface Concentration for Pyridine Adsorbed at the  
Polycrystalline Gold/Aqueous Solution Interface**

by

L. Stolberg, J. Lipkowski, and D.E. Irish

Prepared for Publication

in

Journal of Electroanalytical Chemistry

DTIC  
ELECTE  
JUL 30 1990  
S D<sup>CS</sup> D

Guelph-Waterloo Center for Graduate Work in Chemistry  
Waterloo, Campus  
Department of Chemistry  
University of Waterloo  
Waterloo, Ontario  
Canada, N2L 3G1

July 5, 1990

Reproduction in whole or in part is permitted for  
any purpose of the United States Government

\*This document has been approved for public release  
and sale; its distribution is unlimited.

90 07 00 018

REPORT DOCUMENTATION PAGE

<b>1a REPORT SECURITY CLASSIFICATION</b> Unclassified		<b>1b RESTRICTIVE MARKINGS</b>													
<b>2a SECURITY CLASSIFICATION AUTHORITY</b> Unclassified		<b>3. DISTRIBUTION / AVAILABILITY OF REPORT</b>  Public Release/Unlimited													
<b>2b DECLASSIFICATION / DOWNGRADING SCHEDULE</b>		<b>4. PERFORMING ORGANIZATION REPORT NUMBER(S)</b>  ONR Technical Report #16													
<b>4. PERFORMING ORGANIZATION REPORT NUMBER(S)</b>  ONR Technical Report #16		<b>5. MONITORING ORGANIZATION REPORT NUMBER(S)</b>													
<b>6a NAME OF PERFORMING ORGANIZATION</b> D. E. Irish University of Waterloo	<b>6b OFFICE SYMBOL (If applicable)</b>	<b>7a NAME OF MONITORING ORGANIZATION</b>  Office of Naval Research													
<b>6c. ADDRESS (City, State, and ZIP Code)</b> Department of Chemistry University of Waterloo Waterloo, Ontario, Canada, N2L 3G1		<b>7b. ADDRESS (City, State, and ZIP Code)</b> The Ohio State University, Research Center 1314 Kinnear Road, Room 318 Columbus, Ohio, U.S.A., 43212-1194													
<b>8a NAME OF FUNDING / SPONSORING ORGANIZATION</b>  Office of Naval Research	<b>8b OFFICE SYMBOL (If applicable)</b>	<b>9 PROCUREMENT INSTRUMENT IDENTIFICATION NUMBER</b>  N00014-87-J-1118													
<b>8c ADDRESS (City, State, and ZIP Code)</b> Chemistry Division 800 N. Quincy Street Arlington, VA, U.S.A., 22217-5000		<b>10 SOURCE OF FUNDING NUMBERS</b> <table border="1" style="width:100%; border-collapse: collapse;"> <tr> <td style="width:25%;">PROGRAM ELEMENT NO</td> <td style="width:25%;">PROJECT NO</td> <td style="width:25%;">TASK NO</td> <td style="width:25%;">WORK UNIT ACCESSION NO</td> </tr> <tr> <td> </td> <td> </td> <td> </td> <td> </td> </tr> </table>		PROGRAM ELEMENT NO	PROJECT NO	TASK NO	WORK UNIT ACCESSION NO								
PROGRAM ELEMENT NO	PROJECT NO	TASK NO	WORK UNIT ACCESSION NO												
<b>11 TITLE (Include Security Classification)</b> An Examination of the Relationship Between Surface Enhanced Raman Scattering (SERS) Intensities and Surface Concentration for Pyridine Adsorbed at the Polycrystalline Gold/Aqueous Solution Interface															
<b>12 PERSONAL AUTHOR(S)</b> L. Stolberg, J. Lipkowski, and D.E. Irish															
<b>13a TYPE OF REPORT</b> Technical	<b>13b TIME COVERED</b> FROM 05/89 TO 07/90	<b>14. DATE OF REPORT (Year, Month, Day)</b> 1990-07-05	<b>15. PAGE COUNT</b> 45												
<b>16. SUPPLEMENTARY NOTATION</b>  Submitted to Journal of Electroanalytical Chemistry															
<b>17 COSATI CODES</b> <table border="1" style="width:100%; border-collapse: collapse;"> <thead> <tr> <th style="width:33%;">FIELD</th> <th style="width:33%;">GROUP</th> <th style="width:33%;">SUB-GROUP</th> </tr> </thead> <tbody> <tr> <td> </td> <td> </td> <td> </td> </tr> <tr> <td> </td> <td> </td> <td> </td> </tr> <tr> <td> </td> <td> </td> <td> </td> </tr> </tbody> </table>		FIELD	GROUP	SUB-GROUP										<b>18 SUBJECT TERMS (Continue on reverse if necessary and identify by block number)</b> Surface enhanced Raman scattering from smooth and roughened gold surfaces; correlation between surface concentration, electrochemical measurements, and Raman intensity. <i>JLS</i>	
FIELD	GROUP	SUB-GROUP													
<b>19 ABSTRACT (Continue on reverse if necessary and identify by block number)</b> Surface enhanced Raman scattering (SERS) data are presented for pyridine adsorbed onto both smooth and roughened polycrystalline gold electrode surfaces. It was found that, for smooth surfaces, time independent (stable to within 10% of the initial value) intensities of the totally symmetric ring breathing mode of pyridine (1010 cm <sup>-1</sup> band) could be measured by applying slow oxidation-reduction cycles between each intensity measurement. The potential and concentration dependence of the intensity of the 1010 cm <sup>-1</sup> band was therefore determined. Independently, the isotherms for pyridine adsorption at smooth polycrystalline gold surfaces were obtained using chronocoulometry. The SERS data are compared to the surface concentration data. The SERS intensities are directly proportional to surface concentration at low coverages and deviate, becoming inverse, above half coverage concentrations. Lastly, the effect of surface roughness on the potential and concentration dependence of pyridine SERS was studied. No correlation between the SERS data from rough electrode surfaces and adsorption isotherms determined at a smooth surface was found.															
<b>20 DISTRIBUTION / AVAILABILITY OF ABSTRACT</b> <input checked="" type="checkbox"/> UNCLASSIFIED/UNLIMITED <input type="checkbox"/> SAME AS RPT. <input type="checkbox"/> DTIC USERS		<b>21. ABSTRACT SECURITY CLASSIFICATION</b> Unclassified													
<b>22a NAME OF RESPONSIBLE INDIVIDUAL</b> Dr. Robert J. Nowak		<b>22b. TELEPHONE (Include Area Code)</b> (519) 885-1211, ext. 2500	<b>22c. OFFICE SYMBOL</b>												

An Examination of the Relationship Between Surface Enhanced Raman Scattering (SERS)  
Intensities and Surface Concentration for Pyridine Adsorbed at the  
Polycrystalline Gold/Aqueous Solution Interface

L. Stolberg<sup>1,2</sup>, J. Lipkowski<sup>1</sup> and D.E. Irish<sup>2</sup>

Guelph Waterloo Centre for Graduate Work in Chemistry

<sup>1</sup> Guelph Campus-

University of Guelph,  
Department of Chemistry and Biochemistry,  
Guelph, Ontario, N1G 2W1, Canada.

<sup>2</sup> Waterloo Campus-

University of Waterloo,  
Department of Chemistry,  
Waterloo, Ontario, N2L 3G1, Canada.



Accession For	
NTIS	CRA&I <input checked="" type="checkbox"/>
DTIC	TAB <input type="checkbox"/>
Unannounced	<input type="checkbox"/>
Justification	
By	
Distribution /	
Availability Codes	
Dist	Availability for Special
A-1	

## Abstract

Surface enhanced Raman scattering (SERS) data are presented for pyridine adsorbed onto both smooth and roughened polycrystalline gold electrode surfaces. It was found that, for smooth surfaces, time independent (stable to within 10% of the initial value) intensities of the totally symmetric ring breathing mode of pyridine ( $1010\text{ cm}^{-1}$  band) could be measured by applying slow oxidation-reduction cycles between each intensity measurement. The potential and concentration dependence of the intensity of the  $1010\text{ cm}^{-1}$  band was therefore determined. Independently, the isotherms for pyridine adsorption at smooth polycrystalline gold surfaces were obtained using chronocoulometry. The SERS data are compared to the surface concentration data. The SERS intensities are directly proportional to surface concentration at low coverages and deviate, becoming inverse, above half coverage concentrations. Lastly, the effect of surface roughness on the potential and concentration dependence of pyridine SERS was studied. No correlation between the SERS data from rough electrode surfaces and adsorption isotherms determined at a smooth surface was found.

## Introduction

Understanding the relationship between surface enhanced Raman scattering and surface concentrations of molecules is essential to gaining an understanding of the mechanism of SERS. This relationship has been investigated for pyridine (1-7) as well as for CN (8) at the Ag/vacuum interface, for adsorbates on silver-island films (9,10) and halides and pseudohalides at the silver/electrode surface (11,12). The reason for the relatively few quantitative studies is the lack of surface concentration data for the substrate/adsorbate systems most frequently studied by SERS. This lack of surface concentration data has resulted from the difficulty in determining this parameter for adsorbates on solid electrode surfaces. In order for the SERS technique to be useful to electrochemists as an *in-situ* probe for studying the structure and composition of the inner layer region of the double layer, a knowledge of the relationship between SERS intensities and surface coverage is necessary.

During the past few years we have been investigating the adsorption of pyridine onto both polycrystalline (13) and single crystal (14, 15) gold surfaces using electrochemical techniques. Data such as surface concentrations, the free energies of adsorption and the electrosorption valencies have been determined and pyridine adsorption at the gold surfaces has been described quantitatively. We have also studied the SERS of pyridine adsorbed onto both smooth and roughened polycrystalline gold electrode surfaces. Here we present the first quantitative

correlations between Raman intensities and coverages of the gold surface by adsorbed pyridine molecules.

## Experimental

### i) Solutions

All solutions were prepared from Milli-Q water (Waters). The supporting electrolyte was 0.1 M  $\text{KClO}_4$ .  $\text{KClO}_4$  (ACS Certified from Fisher) was purified by calcinating at 300 °C, recrystallizing twice from Milli-Q water, and then drying. Pyridine (ACS Certified from Fisher) was used without further purification. Pyridine solutions ranging in concentration from  $2 \times 10^{-6}$  M to  $3 \times 10^{-3}$  M were investigated. In the case of the electrochemical experiments these solutions were prepared by spiking a known volume of the electrolyte solution with a small amount of neat pyridine or the appropriate amount of a 0.1 M pyridine stock solution. In the case of the SERS experiments all solutions were prepared from a 0.1 M pyridine stock solution. In both electrochemical and SERS experiments the solutions were purged with argon or nitrogen for at least 1/2 hour before taking measurements and later during experiments argon or nitrogen was passed over the top of the solution.

### ii) Electrodes

#### a) Electrochemical Experiments

The working electrode was a 99.99% pure polycrystalline gold rod formed by inductively heating gold nuggets (Engelhard) under vacuum. Its cross sectional area

was 0.071 cm<sup>2</sup>. The electrode was polished to a mirror finish with progressively finer grades of alumina powder down to the 0.05- μm grade. The electrode was then annealed for 12 hours at 700 °C in a muffle furnace. The counter electrode consisted of a gold coil. An external saturated calomel electrode (SCE) was used as the reference electrode. All potentials reported are relative to the SCE. The temperature was 23 ± 1° C.

Before each experiment the working electrode was cleaned by flaming and quenching with Milli-Q water (16). The hanging electrolyte technique was used to make contact between the gold and the electrolyte solution (17).

#### b) SERS Experiments

The working electrode used in the SERS experiments was made from a polycrystalline gold rod 99.99% pure (Johnston Matthey). The gold rod, whose diameter was 3 mm, was sealed into a Kel-f holder using an epoxy resin (Buehler). Once sealed, the working electrode was polished to a mirror finish with progressively finer grades of alumina ending with the 0.3- μm grade. The counter electrode was a platinum wire and an SCE, separated from the working electrode compartment by a porous glass frit, served as the reference electrode.

SERS measurements were performed on both smooth and roughened gold electrode surfaces. A smooth gold electrode surface was prepared by polishing the gold electrode before each experiment in a 0.3- μm alumina slurry. This was followed by a brief treatment in an ultrasonic water bath in order to remove any alumina

which might have adhered to the surface. Next, the electrode was rinsed with copious amounts of Milli-Q water and transferred to the SERS cell. In-situ cleaning of the surface then followed. This required the use of cyclic voltammetry and involved cycling the electrode potential, using a triangular waveform, between the limits -0.8 V and +1.1 V, at a sweep rate of  $20 \text{ mV s}^{-1}$ . This continuous cycling of the electrode potential usually lasted approximately 2 hours, after which a cyclic voltammogram which reproduced itself from one cycle to the next and displayed the features characteristic of a clean polycrystalline gold electrode surface was observed. In-situ cleaning of the gold surface always took place in a solution containing  $0.1 \text{ M KClO}_4 + x \text{ M pyridine}$  where  $4 \times 10^{-5} \leq x \leq 3 \times 10^{-3}$  and with an anodic limit of +1.1 V and a sweep rate of  $20 \text{ mV s}^{-1}$ . Under such conditions only a few angstroms of the gold surface are removed during the anodic sweep (18).

Shown in Figure 1 are several cyclic voltammograms which illustrate the cleaning procedure. The cyclic voltammograms presented here begin with the second cycle. Notice that as the number of cycles increases the magnitude of the current in the oxide formation region decreases. This behaviour suggests that by using a slow sweep rate we are cleaning our gold surface without roughening it. If the electrode surface was being roughened, we would expect to see an increase in the anodic current due to an increase in the electrode surface area.

Shown in Figure 2 is a scanning electron microscope picture of the SERS electrode after the potential was cycled for two hours using the method described above. In this case in situ cleaning of the electrode surface was carried out in a  $0.1 \text{ M}$

$\text{KClO}_4 + 10^{-3} \text{ M}$  pyridine solution. This photograph corresponds to a 5000 times magnification of the surface. Figure 2 shows the presence of numerous pits whose average diameter is less than  $1 \mu\text{m}$ . In addition scratches, which are the result of mechanical polishing, can also be seen on this photograph. SEM studies on a mechanically polished electrode surface were also carried out. By comparing the photographs of this study (not presented in this publication) with Figure 2, it can be concluded that in situ cleaning does improve the quality of the electrode surface.

An electrode surface which has been prepared using the procedure described above is being referred to as a smooth surface. Of course our surface contains some roughness as Figure 2 clearly shows. However, this electrode was not roughened by the multiple oxidation-reduction cycles described below. This type of surface is a typical SERS substrate and will be referred to as rough.

SERS studies will also be reported for these roughened electrode surfaces. Several methods for preparing such surfaces have been reported in the literature (19-22). The procedure employed in this laboratory is one which has been reported by Gao et al. (19). This particular method involved multiple oxidation-reduction cycles (ORC's) which were carried out in a 0.1 M KCl electrolyte solution. One complete ORC consisted of the following: The electrode potential was first held at -0.3 V for 30 s. Next, the electrode potential was swept from -0.3 V to +1.2 V at a sweep rate of  $1.0 \text{ V s}^{-1}$ . The potential was held at +1.2 V for 1.3 s after which the direction of the potential sweep was reversed. On the reverse cycle the sweep rate was  $0.5 \text{ V s}^{-1}$  with the final potential being -0.3 V. It should be noted that prior to the first cycle the

electrode surface was cathodically cleaned at a potential of -1.4 V for 10 minutes after which the potential was stepped to -0.3 V for 2 minutes in order to remove hydrogen bubbles which were generated during the cathodic cleaning. Hydrogen bubbles were removed from the gold electrode surface by vigorously bubbling nitrogen through the 0.1 M KCl electrolyte solution. Cathodic cleaning was a modification of the procedure reported by Gao et al. (19). Following the last cycle, the roughened gold electrode was rinsed with Milli-Q water and then transferred to the SERS cell. We found that successful roughening of the electrode could only be achieved for freshly polished gold surfaces. It was reported by Gao and coworkers that the most intense SERS signals could be obtained from gold electrode surfaces which had been subjected to 20 - 25 ORC's. In this study as few as 1 cycle and as many as 15 cycles were used, depending on the experiment. Visual inspection of the surface subjected to 15 ORC's showed that it had a pale brown colour while a mirrorlike finish still remained on the surface which had undergone just 1 ORC. Shown in Figure 3 is a SEM photograph (6000 times magnification) of a SERS electrode surface after it was subjected to 15 oxidation-reduction cycles in 0.1 M KCl. This figure shows that the electrode surface after 15 ORC's is very coarse (rough). In addition, tiny nodules of gold are distributed randomly across the surface. These nodules have a diameter approximately equal to 80 nm. According to the electromagnetic theory of SERS , these spheres are active sites. Electrode surfaces which were prepared by potential cycling in 0.1 M KCl will be referred to as rough in the present communication. It was found that the SERS signal due to adsorbed pyridine at ORC-activated surfaces

was stable only for very low laser powers. Thus, a laser power of approximately 8 mW was used in these studies.

### iii) Instrumentation

The details of the instrumentation employed in the electrochemical experiments have been previously reported (13,23-25).

In the case of the SERS experiments, the details of which have been described elsewhere (26), a Dilor OMARS-89 spectrometer equipped with an optical multichannel analyzer and microscope accessory was used. The OMARS-89 spectrometer was operated by using the 1800 groove/mm gratings with two gratings operating in subtractive mode and a third grating dispersing the output onto a 512 diode diode-array detector. For data acquisition the spectrometer was interfaced to an IBM AT computer. The spectra were treated quantitatively by transferring them to a DEC PRO 380 microcomputer where an interactive program called TRICK was available for baseline correction, plotting, and determining the area under a spectral peak.

A Coherent 599 dye laser, pumped with a Coherent Innova 70 argon ion laser operating in the all lines mode, provided laser excitation. The laser dye was DCM (Lambda Physik), which could provide excitation in the wavelength range 610 nm to 710 nm.

For the SERS experiments carried out on a smooth electrode surface the mechanical slit width was 400  $\mu\text{m}$  and the integration time was 1.0 s. The laser power

varied from 50 mW to 225 mW depending on the experiment. In the case of the SERS measurements performed on rough electrode surfaces the mechanical slit width was 300  $\mu\text{m}$ , the exciting line was 680.8 nm, the laser power was 8.0 mW, and the integration time was 2.0 s unless stated otherwise. Particular conditions such as number of accumulations and exciting line wavelength are given in the figure captions.

Scanning electron microscope studies were carried out using a Hitachi S-570 Scanning Electron Microscope. It was operated at a base pressure of  $10^{-7}$  torr to  $10^{-8}$  torr. These pressures were achieved by using a vapour diffusion pump in tandem with a rotary pump. The electrons were accelerated using a voltage of 25 kV. This instrument was equipped with both a high and low detector. Only the low detector could be used due to difficulties in focusing the electron beam on the sample. Thus, the magnification was limited to about 30,000 times.

## Results and Discussion

### i) Time Dependence of the Raman Intensities

Shown in Figure 4 is a SERS spectrum of pyridine adsorbed onto a smooth polycrystalline gold electrode surface which was under an applied electrode potential of -0.4 V (SCE). Two bands at  $1010\text{ cm}^{-1}$  and  $1036\text{ cm}^{-1}$  are visible in the spectral region presented and correspond to the totally symmetric ring breathing mode and trigonal ring breathing mode of pyridine, respectively (27). In this communication we will be concerned with changes in the integrated intensity of the  $1010\text{ cm}^{-1}$  band only.

It was found that the intensity of the  $1010\text{ cm}^{-1}$  band decayed with time. Temporal decay of SERS intensities has been noted previously (28,29). This time dependence was investigated for the system  $\text{Au}/10^{-3}\text{ M pyridine}/0.1\text{ M KClO}_4$ . In order to acquire quantitative data for this and other experiments, the area under the  $1010\text{ cm}^{-1}$  band was determined. This was accomplished by integrating the SERS spectra from  $987\text{ cm}^{-1}$  to  $1025\text{ cm}^{-1}$  and plotting the resulting area, in this case, as a function of time. Prior to integrating, all spectra were baseline corrected by fitting and then subtracting a background spectrum from the spectrum of interest. The background spectrum was obtained, in this case, at  $-0.7\text{ V}$  and did not show any signal due to adsorbed pyridine. Next, a linear baseline correction was made. The spectrum presented in Figure 4 is the result of such a procedure. Shown in Figure 5a-c are plots of the  $1010\text{ cm}^{-1}$  band area versus time for laser powers of  $225\text{ mW}$ ,  $155\text{ mW}$  and  $50\text{ mW}$ , respectively. The data presented here correspond to an electrode potential of  $-0.3\text{ V}$ . It is clear that the signal due to adsorbed pyridine is decaying significantly with time. As Figure 5 indicates, the effect of laser power on the rate of decay of the pyridine signal from gold is quite small in contrast to what we observed for another system, viz., the iodide signal on a roughened copper electrode surface (29). For the latter the effect of laser power was found to have a notable effect.

It was found that if the electrode potential was cycled in between each time-dependent measurement (instead of holding the potential at a fixed value of  $-0.3\text{ V}$ ), the original integrated intensity could be maintained to within 10% of the original value. This is illustrated in Figure 6 which shows a plot of the  $1010\text{ cm}^{-1}$  band area

versus time for the case where the electrode potential is cycled in between measurements (plot a). This involved sweeping the electrode potential, using a triangular waveform, at a rate of  $20 \text{ mV s}^{-1}$  from  $-0.8 \text{ V}$  to  $+1.1 \text{ V}$  and back to  $-0.8 \text{ V}$ . Following the last cycle, the potential was immediately stepped to a value of interest. For comparison the result when no cycling was carried out is also presented (plot b). It is evident from this figure that cycling the electrode potential in between measurements preserves the integrity of the original signal.

The time dependence of SERS intensities has been explained by Pemberton et al. (28) as being the result of a loss of adatom sites which are thought to be active sites in SERS (30). Such a situation may be present in our system. Active sites, such as adatoms, may be generated during the cycling of the electrode potential.

#### ii) Potential Dependence of the Raman Intensity

The potential dependence of the normalized  $1010 \text{ cm}^{-1}$  band area for different bulk pyridine concentrations ranging from  $4 \times 10^{-5}$  to  $3 \times 10^{-3} \text{ M}$  was investigated and the results are presented in Figure 7. Each curve, corresponding to a particular concentration, represents one independent experiment. Differences between each experiment arise not only from differences in the bulk pyridine concentration, but also from irreproducibilities of experimental conditions which include laser power, optical alignment, electrode configuration, etc. In order to compare the results obtained for different concentrations the intensity data were normalized. The normalized band area is defined as  $I_N = I/I_{\text{max}}$  where  $I$  is the area of the band at a

given electrode potential and  $I_{\max}$  is the maximum area observed for a given concentration. The value of the electrode potential at  $I_{\max}$  is defined as  $E_{\max}$ .

Usually an experiment of this type involves the recording of spectra, one after the other, for different applied electrode potentials. A change in the value of the integrated intensity could arise from at least two sources: (a) a change in the applied electrode potential and (b) time. The former may be connected with a change in the surface coverage of pyridine while the latter is a consequence of the time dependence discussed earlier. To eliminate this time dependence slow oxidation-reduction cycles were applied between the measurements, as described above. Prior to the potential dependent measurements, the stability of the  $1010\text{ cm}^{-1}$  band intensity was checked. This involved recording 5 or 6 SERS spectra at an applied electrode potential of  $-0.3\text{ V}$  and subsequently determining the band area, given in Table 1. The electrode potential was cycled in between each measurement given in the table. Although the data in Table 1 show that the  $1010\text{ cm}^{-1}$  band area is stable after just the first measurement, it was found generally that 3 or 4 measurements were required in order for the integrated intensity to be reproduced to within 10%. For the first 5 measurements presented in Table 1, the average deviation is found to be 2.6%. Once certain that intensities reproducible to within 10% could be obtained the potential dependence of the  $1010\text{ cm}^{-1}$  band was investigated by progressively changing the electrode potential from  $0\text{ V}$  to  $-0.75\text{ V}$ . Following the last measurement, which took place at a potential where no signal due to adsorbed pyridine could be detected (i.e.,  $-0.75\text{ V}$ ,  $3 \times 10^{-3}\text{ M}$  pyridine), the electrode potential was stepped, after cycling, to -

0.3 V and a SERS spectrum again recorded (Table 1). This was done as a final check of the stability of the SERS signal. It was found, generally, that the integrated intensity agreed to within 10 - 15% of the value found at the beginning of the experiment although the data presented in Table 1 show a much smaller percentage change. Cycling in between measurements appears to remove the quenching of SERS which occurs at the more extreme negative electrode potentials. This method of cycling in between measurements was employed only for the smooth surface studies.

The curves presented in Figure 7 are bell shaped which is a characteristic feature of many band area-potential curves found in the literature. A strong dependence on the bulk pyridine concentration is also displayed. Both the position of the maximum, as well as the desorption potential, shift in the direction of negative electrode potentials as the bulk pyridine concentration is increased. The desorption potential,  $E_d$ , is defined as the value of the electrode potential at which the SERS signal (or surface concentration) is zero. Values of  $E_d$  can be found in Table 2 along with values of  $E_{max}$ .

### iii) Surface Concentration of Adsorbed Pyridine

Shown in Figure 8 are the surface concentration,  $\Gamma$ -potential curves obtained for pyridine adsorbed onto a polycrystalline gold electrode surface. The surface concentration-potential curves shown here span a range of bulk pyridine concentrations from  $5 \times 10^{-6}$  to  $3 \times 10^{-3}$  M. As Figure 8 indicates, for values of the surface concentration less than  $4.6 \times 10^{-10}$  mol  $\text{cm}^{-2}$ ,  $\Gamma$  depends strongly on both the electrode potential and on the bulk pyridine concentration. These curves shift in the direction

of negative electrode potentials as the bulk pyridine concentration increases; thus the desorption potential shifts in the negative direction with increasing bulk pyridine concentration. For  $\Gamma = 4.6 \times 10^{-10}$  mol cm<sup>-2</sup> a region characterized by a well defined plateau is observed. Here the coverage has become independent of both the pyridine concentration in the bulk of the solution and the electrode potential. Beyond the plateau and near the potential of zero charge (-0.05 V), the surface concentration once again increases and continues to be independent of the bulk pyridine concentration.

Overall the surface concentration-potential curves presented in Figure 8 display a rather complex behaviour. Numerous inflection points, particularly for the higher pyridine concentrations are present. We will show in a future publication that these data can be explained in terms of the superposition of surface concentration-potential curves for the adsorption of pyridine onto low index as well as higher index single crystal planes (i.e., Au(100), Au(110), Au(111) and Au(311)) which make up a polycrystalline surface.

Comparing the SERS data to the surface concentration data for values of  $\Gamma \leq 4.6 \times 10^{-10}$  mol cm<sup>-2</sup>, we see that the two sets of results are in good qualitative agreement. Both sets of data show a strong dependence on the bulk pyridine concentration. Also the desorption potentials, as Table 2 shows, are in excellent agreement. In disagreement with the surface concentration data is the absence of the numerous inflection points from the band area-potential curves. In further disagreement is the decrease in the value of the band area at the more extreme

positive potentials. As Figure 8 shows, the coverage begins to increase and is independent of the bulk pyridine concentration in this region of electrode potentials.

iv) Relationship Between SERS Band Areas and Surface Concentrations

The relationship between the integrated band area,  $I_N$ , and surface concentration of pyridine,  $\Gamma$ , was determined as follows. A band area from graph 7 and a surface concentration from graph 8, corresponding to the same value of the potential were read and sets of such points were plotted against each other to yield Figure 9, for the concentrations  $3 \times 10^{-3}$ ,  $10^{-3}$ ,  $10^{-4}$ , and  $4 \times 10^{-5}$  M pyridine. Consequently the curves in Figure 9a-d correspond to variable electrode potential. The data presented in Figure 9 include values of  $\Gamma \leq 4.6 \times 10^{-10}$  mol cm<sup>-2</sup>. For these values, a strong dependence of  $\Gamma$  on the bulk pyridine concentration is observed (Figure 8). As Figure 9 shows all the curves pass through the origin of the coordinate system and for values of  $\Gamma < 3.2 \times 10^{-10}$  mol cm<sup>-2</sup> the SERS data track the surface concentration data very well. This indicates that the Raman signal arises from adsorbed pyridine molecules. At higher surface concentrations the plots deviate from linearity and pass through a maximum at coverages approximately equal to 2/3 of a monolayer.

Examination of Figure 9 reveals an additional important fact. The maximum value of  $I_N$  occurs for the same value of  $\Gamma$  (viz.  $4.0 \times 10^{-10}$  mol cm<sup>-2</sup>), independent of the bulk pyridine concentration. As the solutions become more concentrated the potential required to achieve this value of  $\Gamma$  becomes more cathodic and in fact shifts some

0.4 V for the concentration change from  $4 \times 10^{-5}$  to  $3 \times 10^{-3}$  M, but to emphasize the point:  $I_N$  maximizes at the same value of coverage, independent of the value of E.

Now in the concentration range of interest  $\Gamma$  is a function of potential E and bulk concentration  $C_b$ , i.e.,  $\Gamma(E, C_b)$ . But the relative integrated Raman intensity  $I_N$  seems to depend only on coverage, and is independent of E. This has implications for the mechanism of SERS operating in this case. Let us consider the evidence.

Following Murray and Bodoff (8) and others for electromagnetic enhancement, the enhanced Raman intensity can be expressed as:

$$I \sim \Gamma \cdot \frac{d\sigma}{d\omega} \cdot F(\Gamma, \omega_L, \omega_R) \cdot S \quad (1)$$

where  $\Gamma$  is the coverage,  $d\sigma/d\Omega$  is the Raman cross section of an adsorbed molecule, F is a function of parameters relating to the electromagnetic field, s is an active surface area fraction,  $\omega_L$  is the laser frequency and  $\omega_R$  is the Raman frequency. Our experiments were performed at constant  $\omega_L$  and  $\omega_R$  and hence equation (1) can be simplified to read:

$$I_{\omega_L, \omega_R} \sim \Gamma \cdot \frac{d\sigma}{d\omega} \cdot F(\Gamma) \cdot S \quad (2)$$

Using equation 2 the normalized band areas plotted in Figures 7 and 9 can be expressed as:

$$I_N = \frac{(I_{\omega_L, \omega_R})_E}{(I_{\omega_L, \omega_R})_{E_{\max}}} = \frac{\Gamma_E \cdot F(\Gamma)_E}{\Gamma_{E_{\max}} \cdot F(\Gamma)_{E_{\max}}} \quad (3)$$

Because the maximum on the integrated intensity curves occurs at the same value of  $\Gamma$  the product  $(\Gamma_{E_{\max}} \cdot F(\Gamma)_{E_{\max}})$  has to have the same value for all pyridine concentrations investigated. Thus the act of normalizing effectively brings the four curves of Figure 9 into correlation with each other. This correlation can be better seen by superimposing the four curves of Figure 9 to yield Figure 10a. This plot in turn can be compared with the plot of  $I_N$  versus  $\Gamma$  at constant electrode potential (Figure 10b). This plot reveals that to a good approximation  $I_N$  is independent of  $E$ . Figures 10a and 10b are superimposable, proving that  $I_N$  is dependent only on coverage  $\Gamma$  and is not dependent on electrode potential. Consequently the potential dependence of integrated Raman intensities observed in Figure 7 is essentially caused by the variation of the surface concentration of adsorbed pyridine molecules. This suggests that for this case the electromagnetic enhancement is the only mechanism that needs to be invoked to rationalize the results, although "chemical" effects are known to contribute to the mechanism for some systems (30-33).

The fact that the Raman intensities,  $I_N$ , pass through a maximum and then decrease at more anodic potentials, a change that is also reflected in Figure 9 at the extreme values of  $\Gamma$ , must be addressed. The Raman intensities primarily display the dependence of the local microscopic field on the electrode surface coverage. Murray and Bodoff (8) predicted that the induced dipoles of adsorbed polarized molecules

depolarize the external field and decrease the magnitude of the local microscopic field at the active site. Consequently their model predicts that Raman intensities will initially vary proportional to coverage and then pass through a maximum at a surface concentration lower than that corresponding to a monolayer. The features displayed in Figures 7 and 9 are consistent with their model.

Mrozek and Otto (34) have recently performed a series of experiments to test the validity of the theory proposed by Murray and Bodoff (8). According to their theory, the local field governs the Raman enhancement of all the vibrational modes. Thus, the intensity variation with increasing coverage should be equal for all modes. Mrozek and Otto investigated the intensity variation for a number of pyridine, benzene, and cyclohexane vibrational modes. These experiments were performed on coldly deposited silver films. For a given adsorbate, the intensity variation with increasing coverage was found to depend on the particular vibrational mode. This is in disagreement with the Murray and Bodoff theory. The Murray and Bodoff theory also predicts that the variation of the local field is governed by the surface concentration and polarizability of the adsorbed molecules. Hence, molecules of roughly the same atomic weight and polarizability should show similar intensity versus coverage relationships. Mrozek and Otto have also tested this experimentally. They found that the totally symmetric ring-breathing-mode for the three molecules studied had quite different coverage dependencies. Once again, this is in disagreement with the theory.

In view of the work of Mrozek and Otto, the above use of the Murray and Bodoff model to explain the SERS of pyridine on polycrystalline gold should be viewed as tentative.

Nonproportional relationships between SERS intensities and surface coverage at high coverages have also been observed for pyridine adsorbed at the Ag/vacuum interface (1-7). Pockrand and Otto (5) reported an increase in the SERS intensity of the  $1006\text{ cm}^{-1}$  vibrational mode of pyridine up to a coverage corresponding to 1 monolayer. A decrease in the SERS intensity then followed with a further increase in the coverage. Eesley (6) found an increase in the SERS intensity up to approximately 0.4 of a monolayer. At higher coverages the intensity decreased and reached a constant value. The results of Rowe et al. (2) were quite similar to those of Eesley (6). The data which we have presented in Figures 7 and 8 are qualitatively similar to the data of Rowe et al. (2), Pockrand (4), Pockrand and Otto (5) and Eesley (6) for coverages in the submonolayer regime. The maximum and subsequent decline in the SERS intensity-coverage plots have also been observed for other adsorbates (8,9). Murray and Bodoff (8) found this bell-shaped SERS intensity-coverage relationship for CN adsorbed onto a Ag island film as did Weitz et al. (9) for p-nitrobenzoate adsorbed onto a similar type of substrate. Recently Kim et al. (10) found the surface enhanced resonance Raman scattering (SERRS) intensity of a cyanine dye dispersed in Langmuir-Blodgett monolayers in contact with a silver island film to also be of this form. The similarity of our data to the data obtained at the metal/gas or vacuum

interfaces can be explained by the dipole depolarization effect which is operating in all of these systems.

v) Effect of Surface Roughness

In most of the electrochemical SERS studies reported in the literature, roughened electrode surfaces were used as the substrate. It was of interest to see how the SERS data for pyridine adsorbed onto roughened gold electrode surfaces compared to the SERS data obtained for pyridine adsorbed onto a smooth surface.

Presented in Figure 11 are  $1010\text{ cm}^{-1}$  band area-potential curves which have been obtained for roughened (1, 7 and 15 ORC's) gold electrodes. The strength of the SERS signal is markedly greater than that from the smooth surfaces reported above, and thus lower laser powers were used. The solution composition in each case was  $10^{-3}\text{ M}$  pyridine,  $0.1\text{ M KClO}_4$ . As this figure shows, surface roughness has a profound effect on the form of the band area-potential curve. In going from a mildly rough surface (1 ORC) to one which has been roughened by applying 15 oxidation-reduction cycles, we see that both the position of the maximum, as well as the potential at which the Raman signal disappears, shift dramatically in the direction of negative electrode potentials. However, the position of the maximum eventually becomes invariant as indicated by the coincidence of the maxima observed from the curves corresponding to 7 and 15 ORC's. The potential at which the Raman signal disappears as well as the position of the maxima are listed in Table 3 for both the rough and smooth electrode surfaces. As Figure 11 shows, the overall effect of surface

roughness is to extend the potential region over which the Raman signal for the pyridine molecules can be observed. For these rough electrode surfaces pyridine adsorption appears to overlap hydrogen evolution which begins at potentials negative of -0.8 V in the electrolyte solution described above. Gao et al. (19) have also reported data which show strong SERS signals from pyridine on roughened gold surfaces in the region of electrode potentials where hydrogen evolution takes place.

It was of further interest to see if the band area-potential curves for roughened electrodes displayed a dependence on the bulk pyridine concentration. Shown in Figure 12 are band area-potential curves for various bulk pyridine concentrations ranging from  $10^{-4}$  M to  $3 \times 10^{-3}$  M. The electrode surfaces used in these studies were roughened using only 1 ORC. The reason why only 1 ORC was used in this study is related to reproducibility. It was found that the reproducibility of the band area-potential curve was very poor for electrode surfaces subjected to multiple oxidation-reduction cycles compared with surfaces roughened using only 1 ORC. As this figure indicates, there is a strong dependence on the bulk pyridine concentration. Both the position of the maximum as well as the desorption potential depend on the bulk pyridine concentration. In accordance with the surface concentration data, these curves shift in the direction of negative electrode potentials as the concentration of pyridine in the bulk of the solution is increased.

The band area-potential curve presented in Figure 11 for a surface which has been roughened by applying 15 ORC's suggests that pyridine desorption is taking place at an electrode potential of -1.5 V. Furthermore, this curve displays a maximum

at a potential of -0.6 V were the electrochemical data suggest that there are very few pyridine molecules present on the gold surface. This discrepancy between the SERS data and the electrochemical data is illustrated in Figure 13 which shows a plot of  $I_N$  versus  $\Gamma$  for an electrode surface roughened by applying 15 ORC's. As this figure shows, strong SERS signals are measured where the surface coverage was found to be zero. These differences between the SERS data and the electrochemical data can be explained in terms of the classical (EM) enhancement effect which is operative on a rough surface and is responsible in large part for the overall observed SERS intensity (35). The EM effect has both a short as well as a long range nature. This implies that pyridine molecules which are in direct contact with the surface, as well as those which are present in the second, third, etc., layers, can give rise to a SERS signal. Thus, the data in Figure 11 can be explained in terms of SERS from pyridine molecules which are not necessarily in direct contact with the gold electrode surface. The electrochemical data give us information only about those pyridine molecules which are in direct contact with the surface.

### Summary and Conclusions

We have presented SERS data for pyridine adsorbed onto both smooth and rough polycrystalline gold electrode surfaces. For the smooth surface both the time dependence and potential dependence of the  $1010\text{ cm}^{-1}$  band were examined. The time dependence of pyridine SERS was found to be essentially independent of the laser power. However, it could be controlled during an experiment by cycling the

electrode potential in between each intensity measurement. With this technique, the integrated intensity could be maintained to within 10 - 15% of the original  $t = 0$  s value. The potential dependence of pyridine SERS was found to be strongly dependent on the bulk pyridine concentration. These data were compared to the surface concentration data which were obtained using electrochemical techniques. The surface concentration data also displayed a strong dependence on the bulk pyridine concentration. For both low and moderate coverages, the SERS data were found to track the surface concentration data very well. The SERS data were explained in terms of a model which takes into account the depolarising effect which the adsorbed molecules have on the local electromagnetic field. The integrated SERS intensity is directly proportional to the surface coverage for low coverages. At higher coverages the SERS intensity-coverage relationship becomes inverse. This curving down at high coverages is commonly observed in SERS.

The effect of surface roughness was also investigated. It was found that the band area-potential curve showed both a qualitative and quantitative dependence on the degree of surface roughness. The data from such surfaces did not give an accurate description of pyridine adsorption onto polycrystalline gold.

Acknowledgement This work was supported by grants from the Natural Sciences and Engineering Research Council of Canada and the Office of Naval Research (USA).

## References

1. R.R. Smardzewski, R.J. Colton and J.S. Murday, Chem. Phys. Lett., 68 (1979) 53.
2. J.E. Rowe, C.V. Shank, D.A. Zwemer and C.A. Murray, Phys. Rev. Lett., 44 (1980) 1770.
3. D. A. Zwemer, C.V. Shank and J.E. Rowe, Chem. Phys. Lett., 73 (1980) 201.
4. I. Pockrand, Chem. Phys. Lett., 92 (1982) 509.
5. I. Pockrand and A. Otto, Solid State Commun., 35 (1980) 861.
6. G.L. Eesley, Phys. Lett., 81A (1981) 193.
7. P.N. Sanda, J.M. Warlaumont, J.E. Demuth, J.C. Tsang, K. Christman and J.A. Bradley, Phys. Rev. Lett., 45 (1980) 1519.
8. C.A. Murray and S. Bodoff, Phys. Rev. B, 32 (1985) 671.
9. D.A. Weitz, S. Garoff, J.I. Gersten and A. Nitzan, J. Chem. Phys., 78 (1983) 5324.
10. J-H. Kim, T.M. Cotton, R.A. Uphaus and D. Möbius, J. Phys. Chem., 93 (1989) 3713.
11. M.J. Weaver, J.T. Hupp, F. Barz, J.G. Gordon II and M.R. Philpott, J. Electroanal Chem., 160 (1984) 321.
12. H. Wetzal, H. Gerischer and B. Pettinger, Chem. Phys. Lett., 78 (1981) 392.
13. L. Stolberg, J. Richer, J. Lipkowski and D.E. Irish, J. Electroanal. Chem. 207 (1986) 213.
14. L. Stolberg, J. Lipkowski and D.E. Irish, J. Electroanal. Chem., 238 (1987) 333.
15. L. Stolberg, J. Lipkowski and D.E. Irish, J. Electroanal. Chem. in press.

16. J. Clavilier, *J. Electroanal. Chem.*, 107 (1980) 211.
17. D. Dickertmann, J.W. Shultze and F.D. Koppitz, *Electrochim Acta*, 21 (1976) 967.
18. D. Dickertmann, J.W. Schultze and K.W. Vetter, *J. Electroanal. Chem.*, 55 (1974) 429.
19. P. Gao, D. Gosztola, L-W. H. Leung and M. J. Weaver, *J. Electroanal. Chem.*, 233 (1987) 211.
20. C.C. Busby and J.A. Creighton, *J. Electroanal. Chem.*, 140 (1982) 379.
21. H. Baltruschat, N. Staud and J. Heitbaum, *J. Electroanal. Chem.*, 239 (1988) 361.
22. R. Holze, *Surf. Sci.*, 202 (1988) L612.
23. A. Iannelli, J. Richer and J. Lipkowski, *Langmuir*, 5 (1989) 466.
24. J. Richer, L. Stolberg and J. Lipkowski, *Langmuir*, 2 (1986) 630.
25. A. Hamelin, S. Morin, J. Richer and J. Lipkowski, *J. Electroanal. Chem.* 272 (1989) 241.
26. D.A. Guzonas, D.E. Irish and G.F. Atkinson, *Langmuir*, 5 (1989) 787.
27. F.R. Dollish, W.G. Fateley and F.F. Bentley, "Characteristic Raman Frequencies of Organic Compounds", John Wiley and Sons Inc., New York, 1974, p 264.
28. J.E. Pemberton, A.L. Guy, R.L. Sobocinski, D.D. Tuschel and N.A. Cross, *Surf. Sci.*, 32 (1988) 33.
29. D.E. Irish, L. Stolberg and D.W. Shoesmith, *Surf. Sci.*, 158 (1985) 238.

30. A. Otto, I. Pockrand, J. Billman and C. Pettenkofer in "Surface Enhanced Raman Scattering", R.K. Chang and T.E. Furtak, Eds., Plenum Press, New York, 1982, p 147-172.
31. A. Otto in "Light Scattering in Solids IV ", M. Cardona and G. Guntheredt, Eds., Topics in Applied Physics, Vol. 54, Springer, Berlin (1984), p. 289.
32. A. Otto, Proc. 6th Int. Conf. on Surface and Colloid Science, in Colloids and Surfaces 38 (1989) 27, and references therein.
33. D. Guzonas, D.E. Irish and G.F. Atkinson, Langmuir, in press.
34. I. Mrozek and A. Otto, J. Elec. Spectrosc. and Rel. Phenomenon 45 (1987) 143.
35. M. Moskovits, Rev. Mod. Phys., 57 (1985) 783.

## Figures

### Figure 1.

Cyclic voltammograms illustrating the in-situ cleaning of a smooth gold electrode in a solution containing  $3 \times 10^{-10}$  M pyridine, 0.1 M  $\text{KClO}_4$ . The second, third, fourth and twelfth cycle are indicated. Sweep rate =  $20 \text{ mV s}^{-1}$ .

### Figure 2.

Scanning electron microscope photograph of the SERS electrode surface after in situ cleaning. The electrode potential was cycled for two hours in a solution containing 0.1 M  $\text{KClO}_4$  +  $10^{-3}$  M pyridine.

### Figure 3.

Scanning electron microscope photograph of the SERS electrode surface after the application of 15 oxidation-reduction cycles. The electrolyte was 0.1 M KCl.

### Figure 4.

SERS spectrum of pyridine adsorbed onto a smooth polycrystalline gold electrode surface from a solution containing  $3 \times 10^{-3}$  M pyridine, 0.1 M  $\text{KClO}_4$ . Exciting line - 680.471 nm, laser power - 150 mW, 90 accumulations.

### Figure 5.

Plots of the  $1010 \text{ cm}^{-1}$  band area versus time for laser powers of: (a) 225 mW; (b) 155 mW; (c) 50 mW. The solution composition is  $10^{-3}$  M pyridine, 0.1 M  $\text{KClO}_4$  and the applied electrode potential is -0.3 V. Exciting line - 667.983 nm, 90 accumulations.

Figure 6.

Plots illustrating the time dependence of the  $1010\text{ cm}^{-1}$  band for: (●) with cycling in between measurements and (■) without cycling in between measurements. Exciting line -  $675.5\text{ nm}$ , laser power -  $150\text{ mW}$ , 150 accumulations.

Figure 7.

Plots of  $I_N$  versus  $E$  for the following bulk pyridine concentrations: (●)  $4 \times 10^{-5}\text{ M}$ ; (■)  $10^{-4}\text{ M}$ ; (▲)  $10^{-3}\text{ M}$ ; (○)  $3 \times 10^{-3}\text{ M}$ . Exciting line -  $680.471\text{ nm}$ , laser power -  $150\text{ mW}$ , 90 accumulations.

Figure 8.

Surface concentration versus potential curves for the following bulk pyridine concentrations: (1)  $3 \times 10^{-3}\text{ M}$ ; (2)  $10^{-3}\text{ M}$ ; (3)  $5 \times 10^{-4}\text{ M}$ ; (4)  $3 \times 10^{-4}\text{ M}$ ; (5)  $10^{-4}\text{ M}$ ; (6)  $3 \times 10^{-5}\text{ M}$ ; (7)  $10^{-5}\text{ M}$ ; (8)  $5 \times 10^{-6}\text{ M}$ .

Figure 9.

Plots of  $I_N$  versus  $\Gamma$  for the following bulk pyridine concentrations: (a)  $3 \times 10^{-3}\text{ M}$ ; (b)  $10^{-3}\text{ M}$ ; (c)  $10^{-4}\text{ M}$ ; (d)  $4 \times 10^{-5}\text{ M}$ .

Figure 10.

Plots illustrating the relationship between  $I_N$  and  $\Gamma$  for: (a) superimposition of the data presented in Figure 7. Data for the following bulk pyridine concentrations are shown: (○)  $3 \times 10^{-3}\text{ M}$ ; (●)  $10^{-3}\text{ M}$ ; (□)  $10^{-4}\text{ M}$ ; (■)  $4 \times 10^{-5}\text{ M}$  and (b) constant electrode potential. Data for the following electrode potentials are presented: (▼)  $-0.65\text{ V}$ ; (▽)  $-0.6\text{ V}$ ; (○)  $-0.55\text{ V}$ ; (●)  $-0.5\text{ V}$ ; (□)  $-0.45\text{ V}$ ; (■)  $-0.4\text{ V}$ ; (▲)  $-0.35\text{ V}$ ; (△)  $-0.3\text{ V}$ ; (◇)  $-0.25\text{ V}$ ; (◆)  $-0.2\text{ V}$ .

Figure 11.

$I_N$  versus E curves depicting the effect of surface roughness. (O) 1 ORC, 125 accumulations; (□) 7 ORC's, integration time - 3.0 s, 50 accumulations; (▲) 15 ORC's, 50 accumulations.

Figure 12.

Normalized band area versus electrode potential curves illustrating the effect of bulk pyridine concentration for a gold electrode subjected to 1 oxidation-reduction cycle. (●)  $10^{-4}$  M, 3.0 s integration time; (■)  $5 \times 10^{-4}$  M; (▲)  $10^{-3}$  M; (◆)  $3 \times 10^{-3}$  M.  $5 \times 10^{-4}$  M - 150 accumulations, all other concentrations 125 accumulations.

Figure 13.

Plot showing the relationship between  $I_N$  and  $\Gamma$  for a surface subjected to 15 oxidation-reduction cycles. The bulk pyridine concentration is  $10^{-3}$  M.

Table 1.

The stability of the integrated  $1010\text{ cm}^{-1}$  band area during the course of a potential dependent experiment. Cycling was carried out between each measurement.

E / V	$1010\text{ cm}^{-1}$ Band Area
-0.3	1418
-0.3	1473
-0.3	1386
-0.3	1477
-0.3	1485
0	1071
-0.1	1219
-0.2	1375
-0.3	1437
-0.4	1546
-0.5	1437
-0.6	937
-0.7	59
-0.75	0
-0.3	1433

Table 2.

Desorption potentials,  $E_d$ , as determined from the SERS and electrochemical measurements and the potential of the intensity maximum.

$C / \text{mol dm}^{-3}$	$E_d / \text{V}$ (SERS)	$E_d / \text{V}$ (Electrochemical)	$E_{\text{max}} / \text{V}$
$3 \times 10^{-3}$	-0.75	-0.75	-0.40
$10^{-3}$	-0.70	-0.70	-0.37
$10^{-4}$	-0.55	-0.60	-0.24
$4 \times 10^{-5}$	-0.50	-0.55	-0.16

Table 3.

The effect of surface roughness (increasing with number of cycles) on the desorption potential,  $E_d$ , and the potential of the intensity maximum,  $E_{max}$ .

Number of Cycles	$E_d / V$ (SERS)	$E_{max} / V$
0	-0.70	-0.37
1	-1.0	-0.45
7	-1.1	-0.60
15	-1.5	-0.60

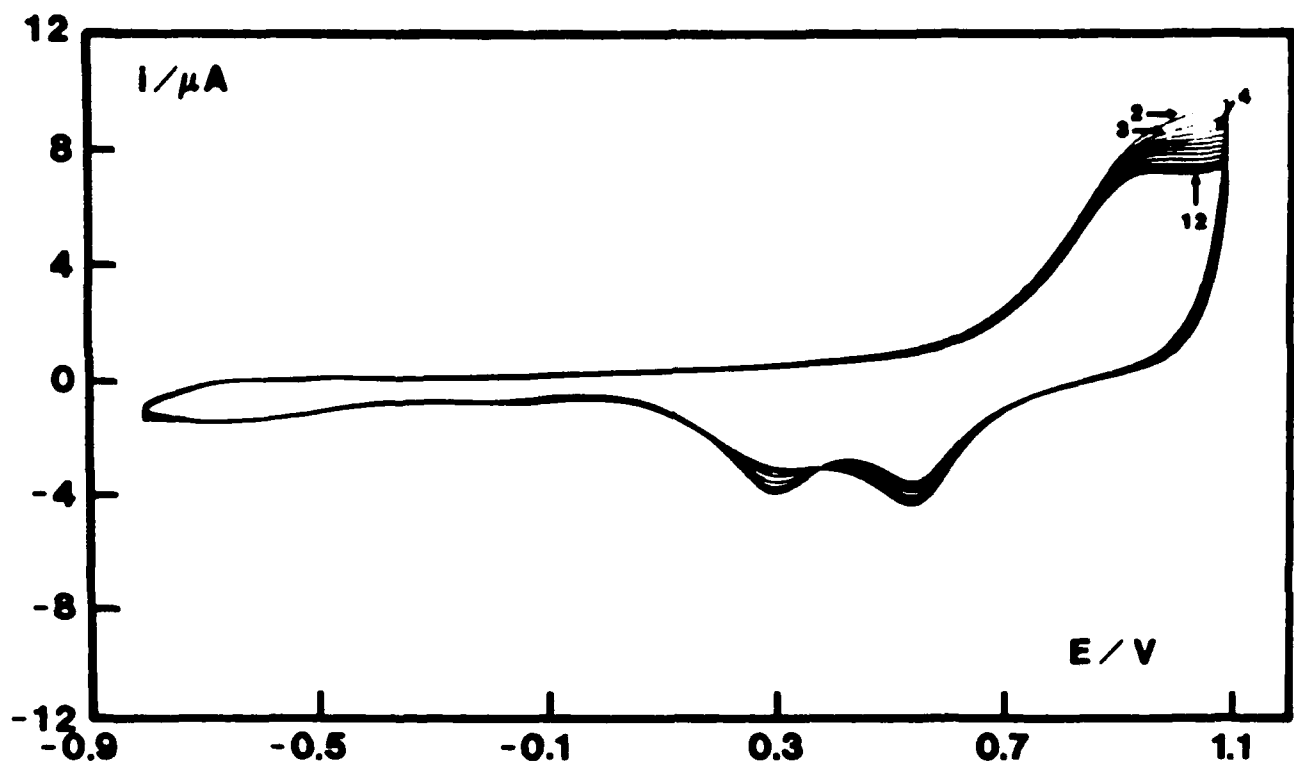


Figure 1.

Cyclic voltammograms illustrating the in-situ cleaning of a smooth gold electrode in a solution containing  $3 \times 10^{-10}$  M pyridine, 0.1 M  $\text{KClO}_4$ . The second, third, fourth and twelfth cycle are indicated. Sweep rate =  $20 \text{ mV s}^{-1}$ .

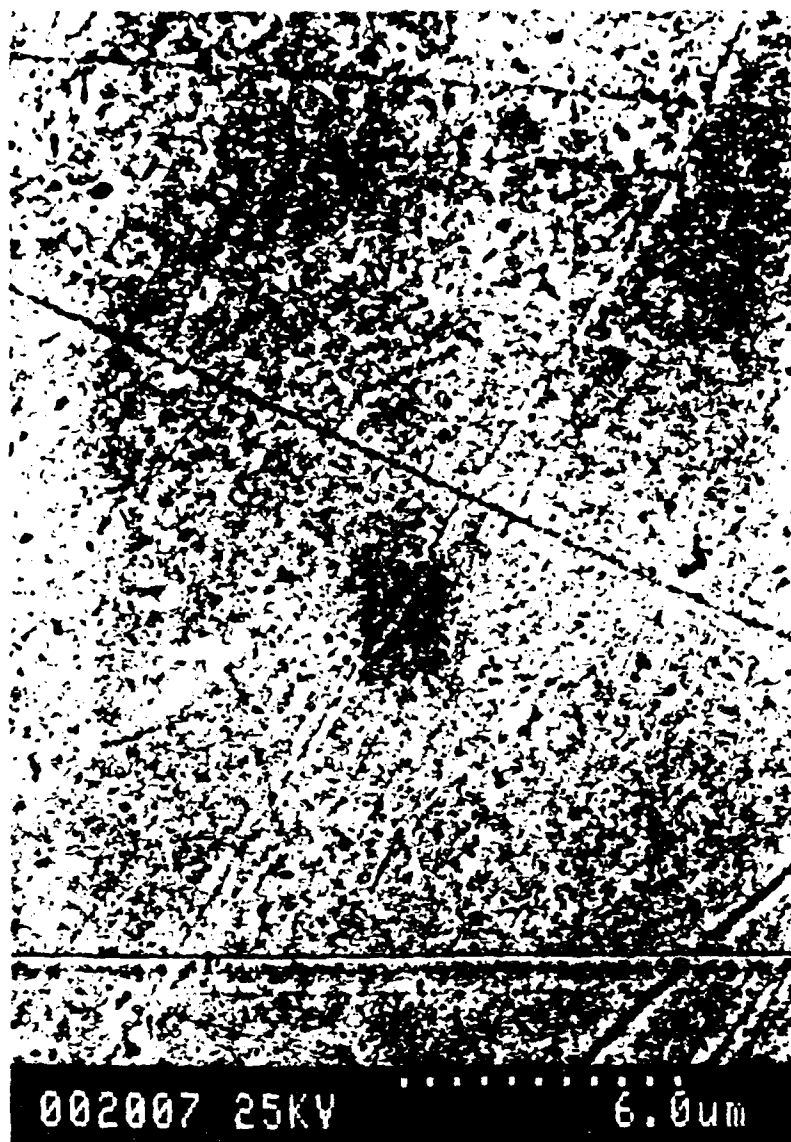


Figure 2.

Scanning electron microscope photograph of the SERS electrode surface after in situ cleaning. The electrode potential was cycled for two hours in a solution containing 0.1 M  $\text{KClO}_4$  +  $10^{-3}$  M pyridine.

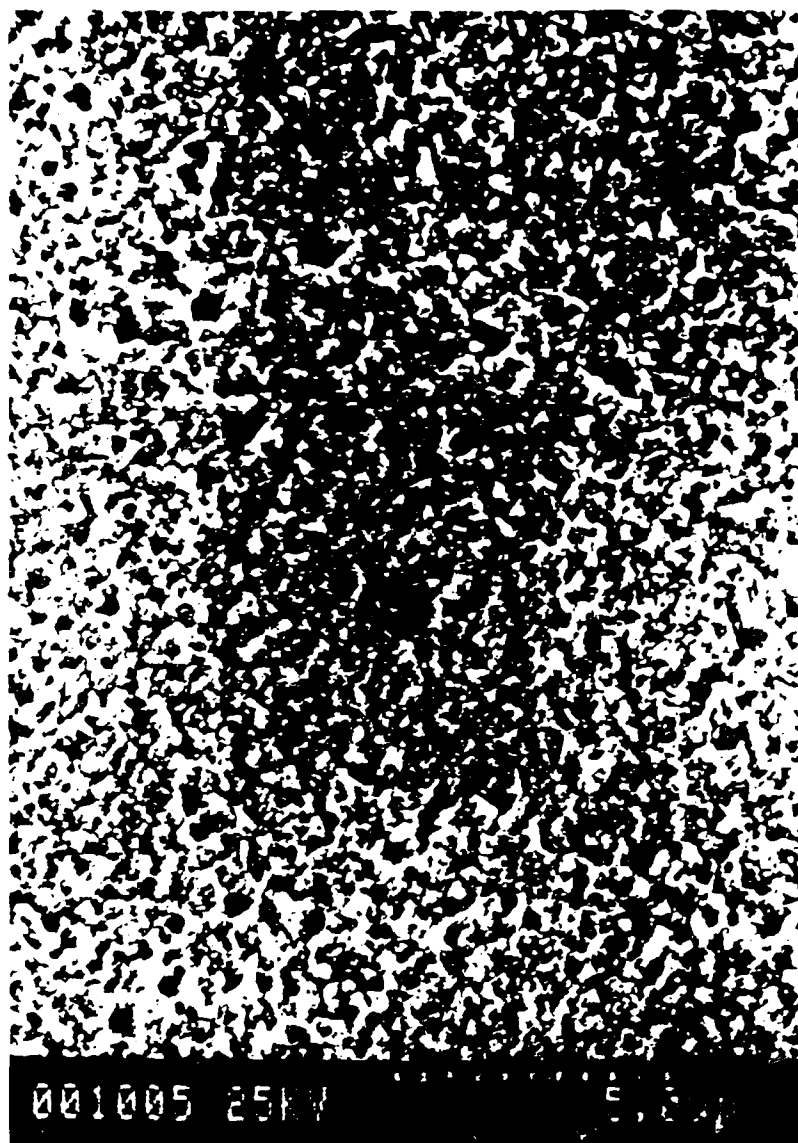
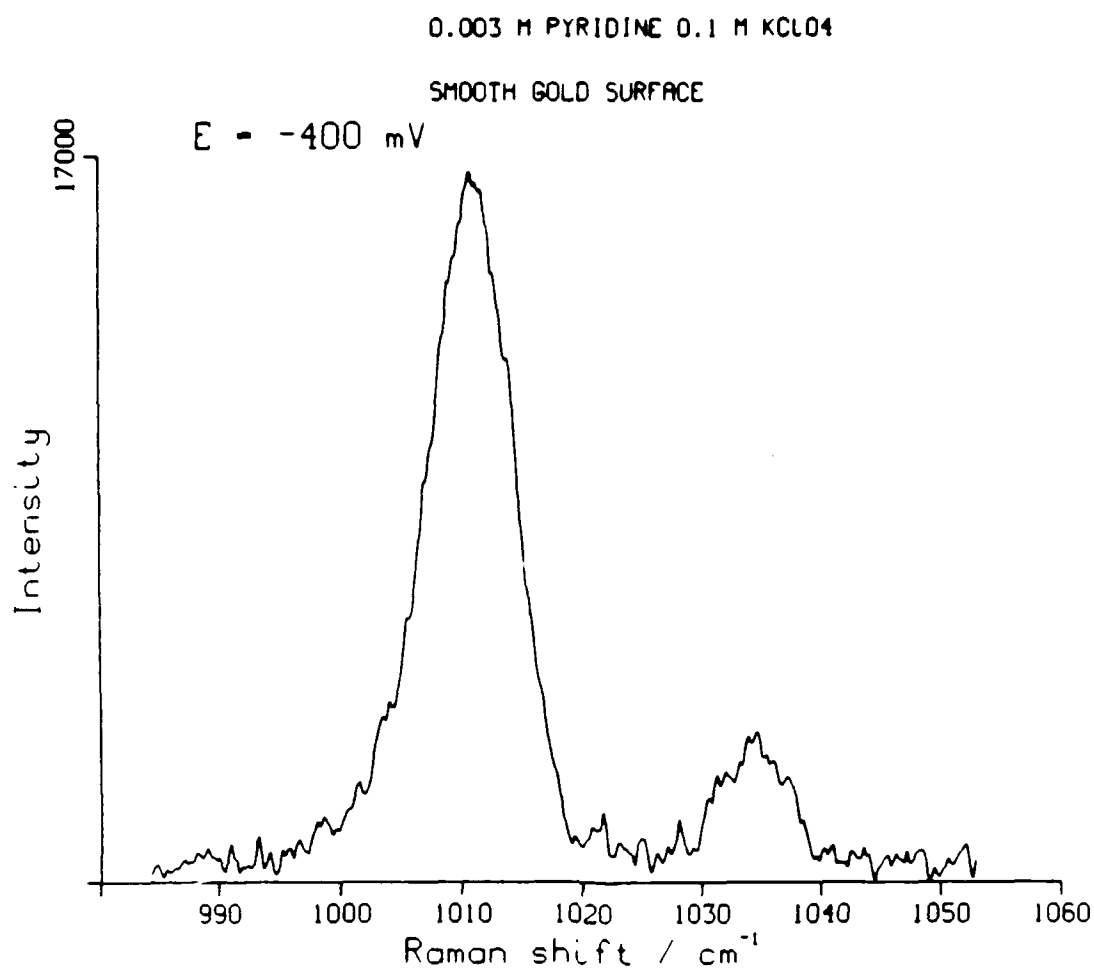


Figure 3.

Scanning electron microscope photograph of the SERS electrode surface after the application of 15 oxidation-reduction cycles. The electrolyte was 0.1 M KCl.



**Figure 4.**

SERS spectrum of pyridine adsorbed onto a smooth polycrystalline gold electrode surface from a solution containing  $3 \times 10^{-3}$  M pyridine, 0.1 M KClO<sub>4</sub>. Exciting line - 680.471 nm, laser power - 150 mW, 90 accumulations.

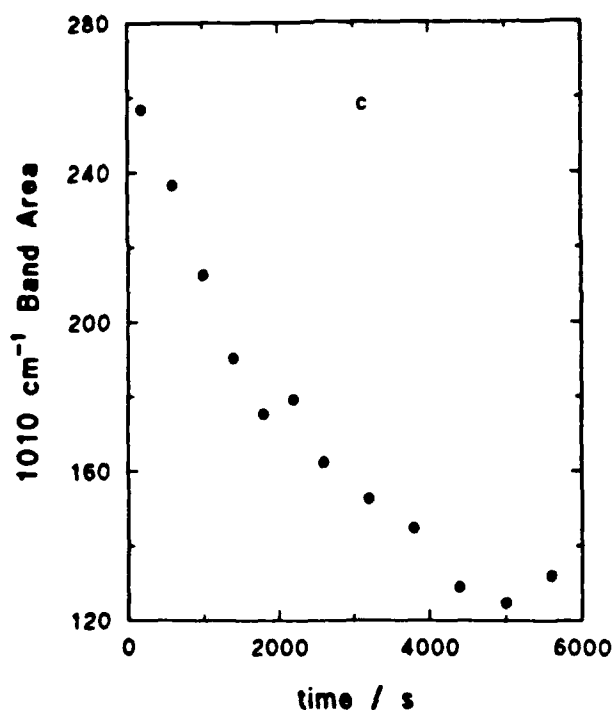
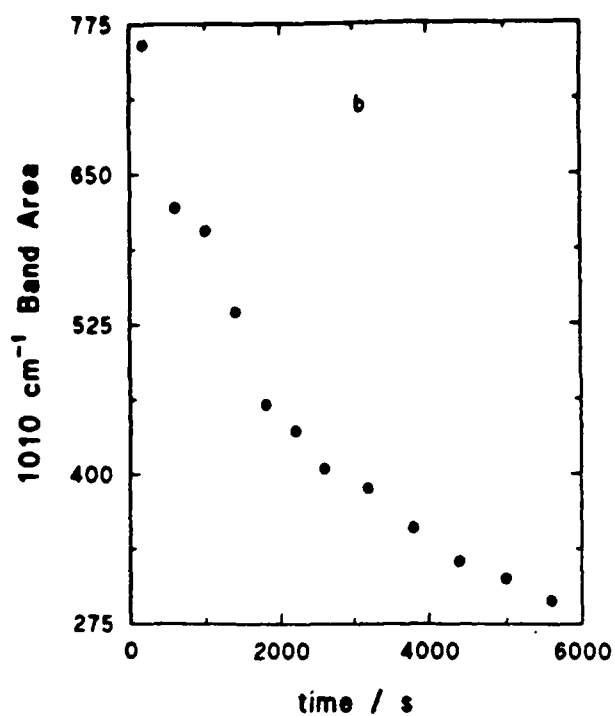
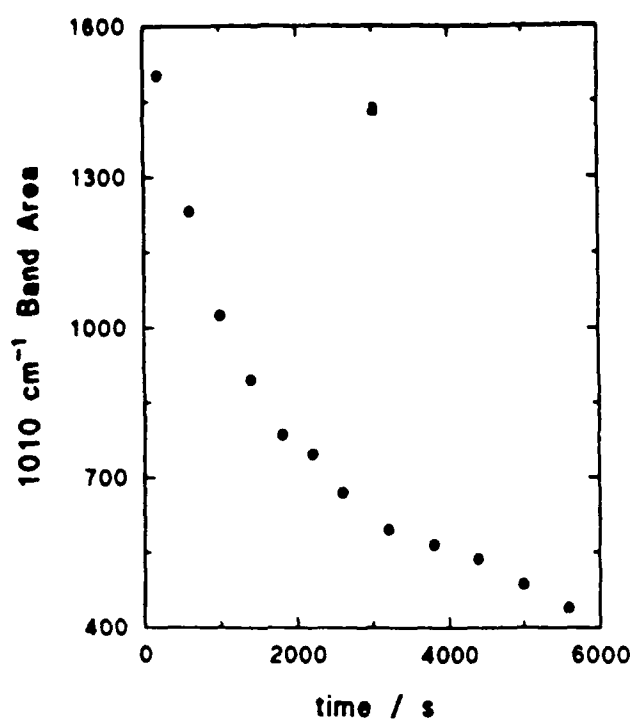


**Figure 5.**

Plots of the  $1010\text{ cm}^{-1}$  band area versus time for laser powers of: (a) 225 mW; (b) 155 mW; (c) 50 mW. The solution composition is  $10^{-3}\text{ M}$  pyridine,  $0.1\text{ M}$   $\text{KClO}_4$  and the applied electrode potential is  $-0.3\text{ V}$ . Exciting line -  $667.983\text{ nm}$ , 90 accumulations.

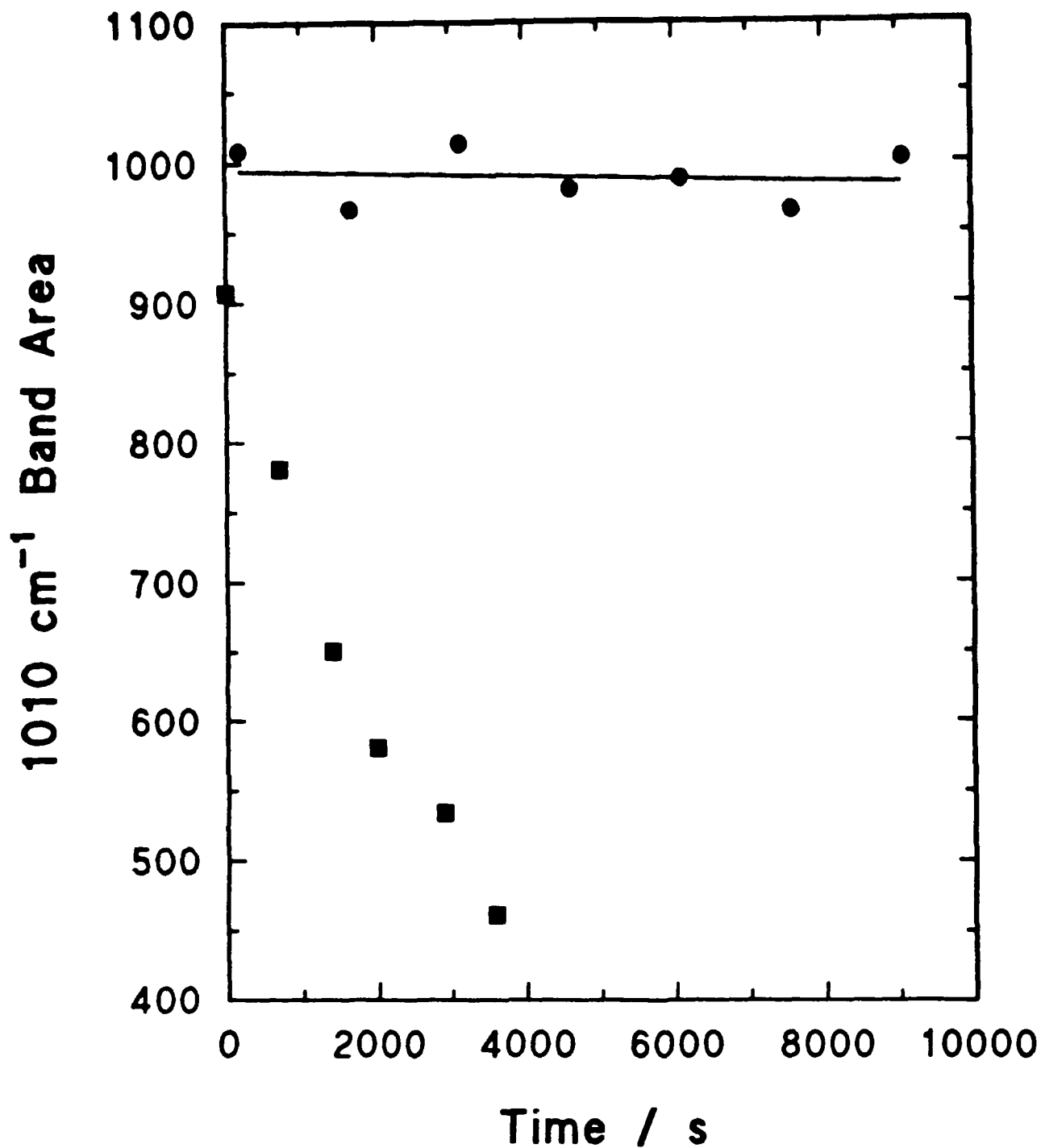


Figure 6.

Plots illustrating the time dependence of the  $1010\text{ cm}^{-1}$  band for: (●) with cycling in between measurements and (■) without cycling in between measurements. Exciting line -  $675.5\text{ nm}$ , laser power -  $150\text{ mW}$ , 150 accumulations.

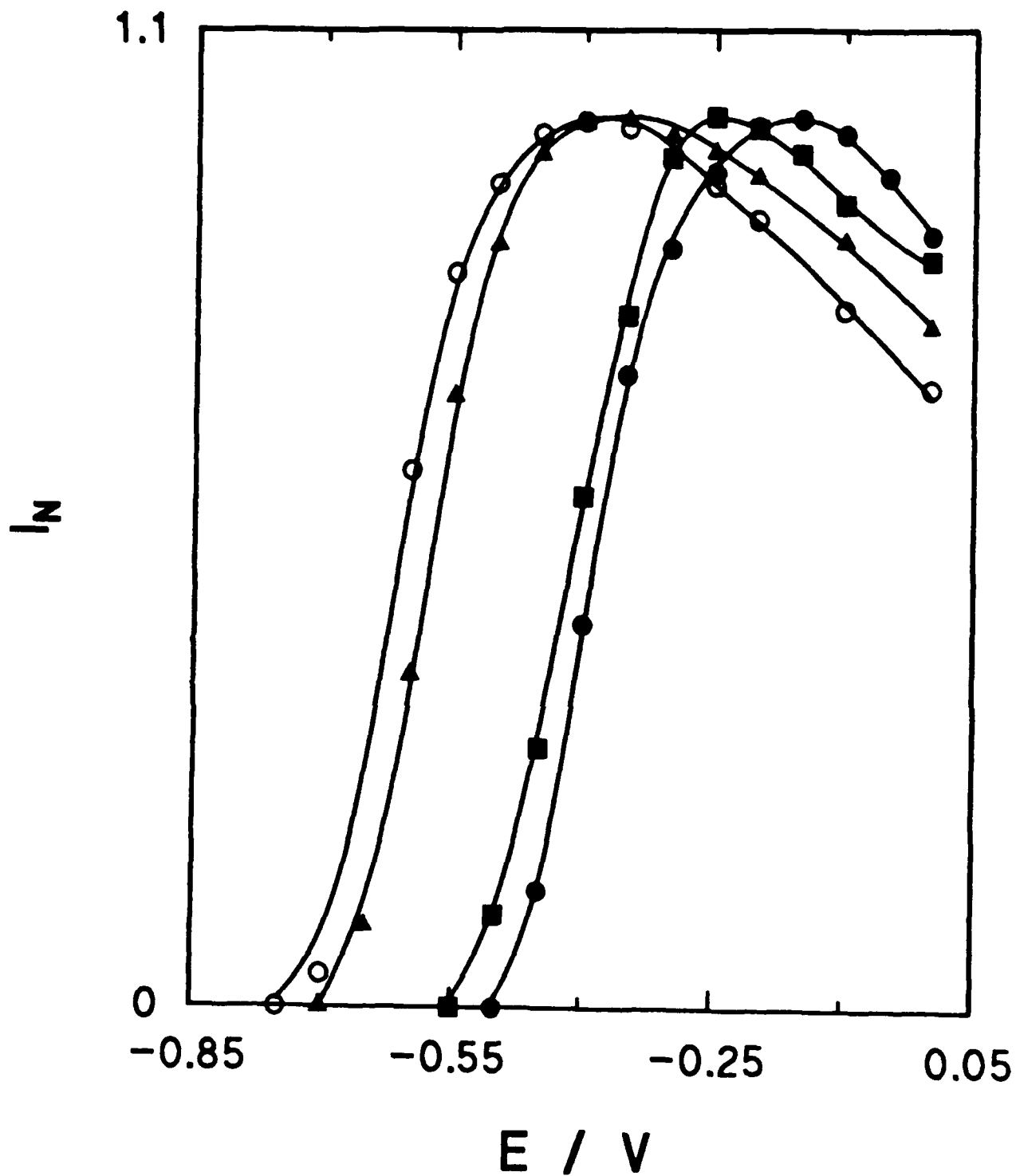


Figure 7.

Plots of  $I_N$  versus  $E$  for the following bulk pyridine concentrations: (●)  $4 \times 10^{-5}$  M; (■)  $10^{-4}$  M; (▲)  $10^{-3}$  M; (○)  $3 \times 10^{-3}$  M. Exciting line - 680.471 nm, laser power - 150 mW, 90 accumulations.

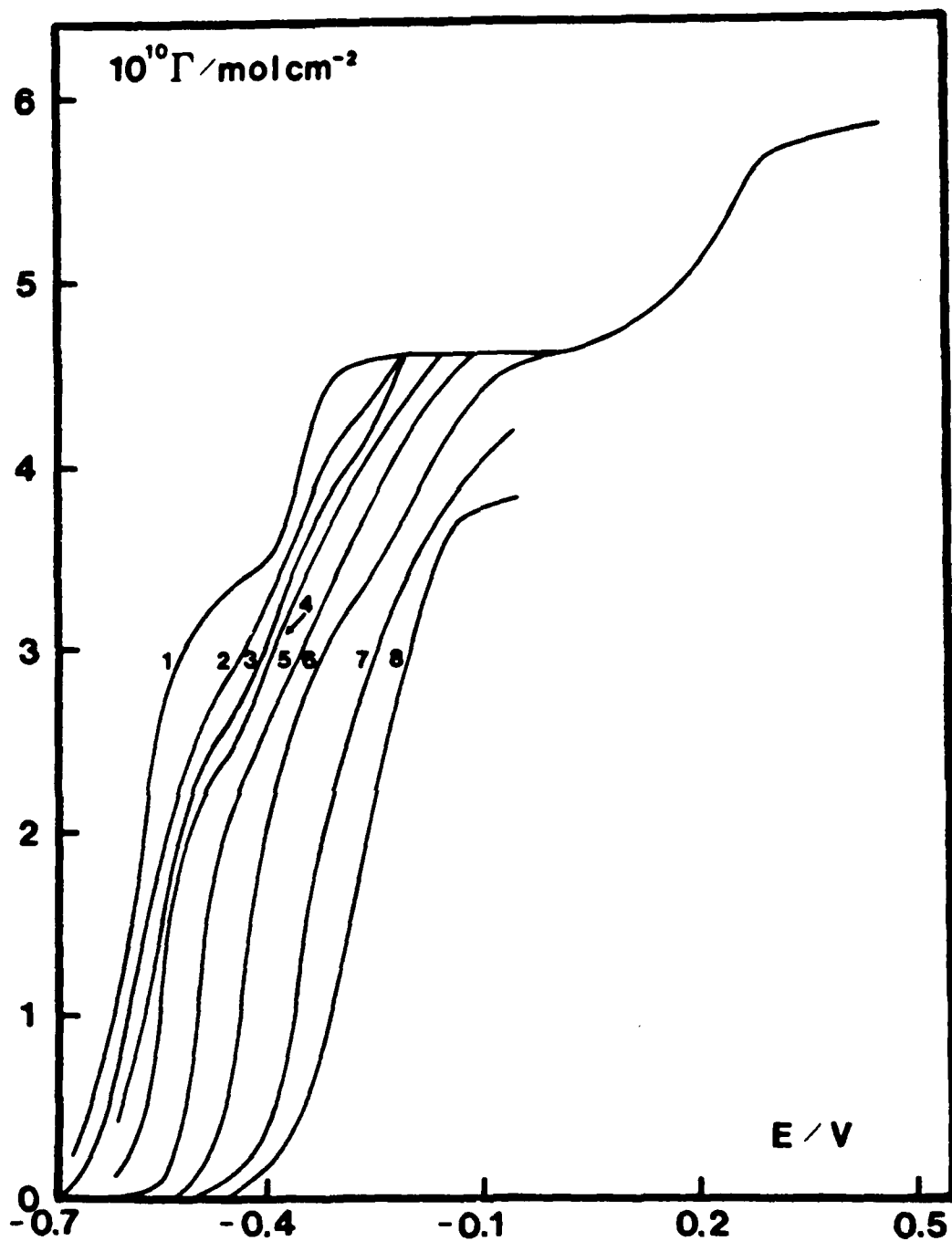


Figure 8.

Surface concentration versus potential curves for the following bulk pyridine concentrations: (1)  $3 \times 10^{-3}$  M; (2)  $10^{-3}$  M; (3)  $5 \times 10^{-4}$  M; (4)  $3 \times 10^{-4}$  M; (5)  $10^{-4}$  M; (6)  $3 \times 10^{-5}$  M; (7)  $10^{-5}$  M; (8)  $5 \times 10^{-6}$  M.

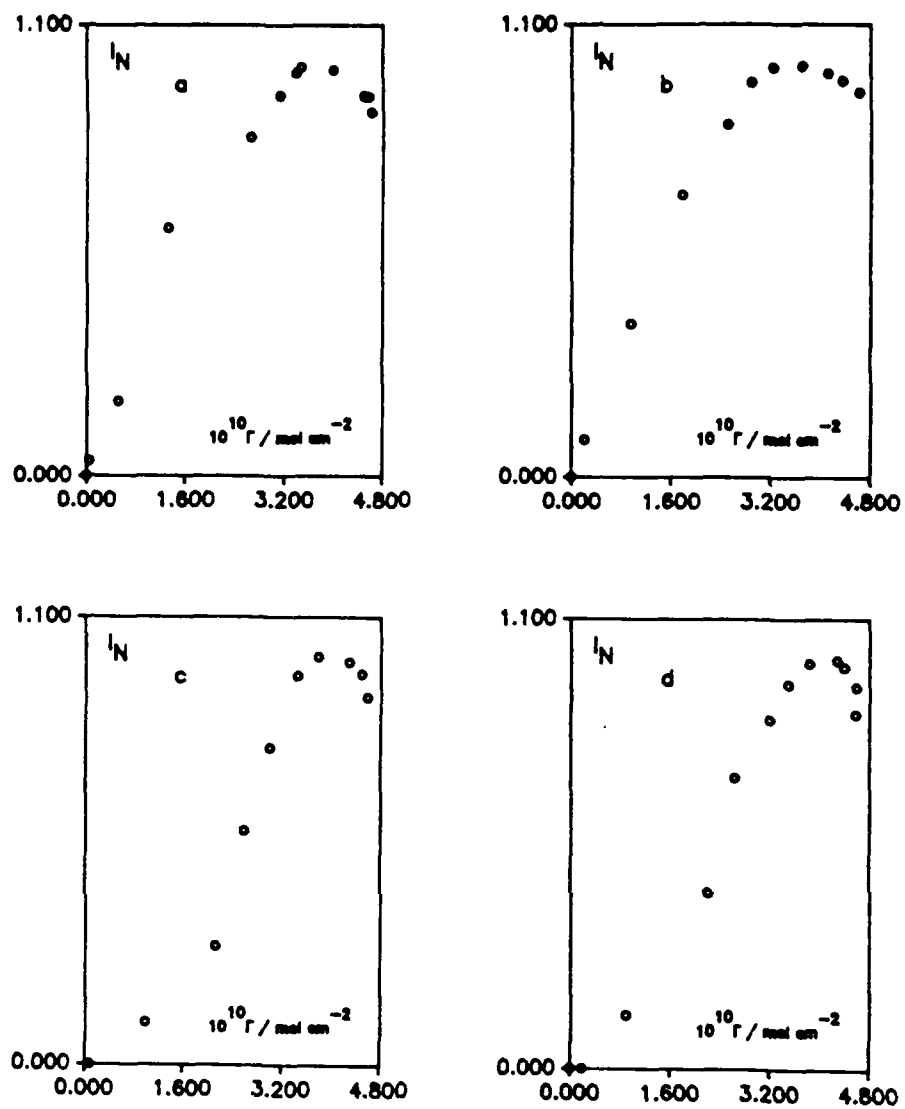


Figure 9.

Plots of  $I_N$  versus  $\Gamma$  for the following bulk pyridine concentrations: (a)  $3 \times 10^{-3} \text{ M}$ ;

(b)  $10^{-3} \text{ M}$ ; (c)  $10^{-4} \text{ M}$ ; (d)  $4 \times 10^{-5} \text{ M}$ .

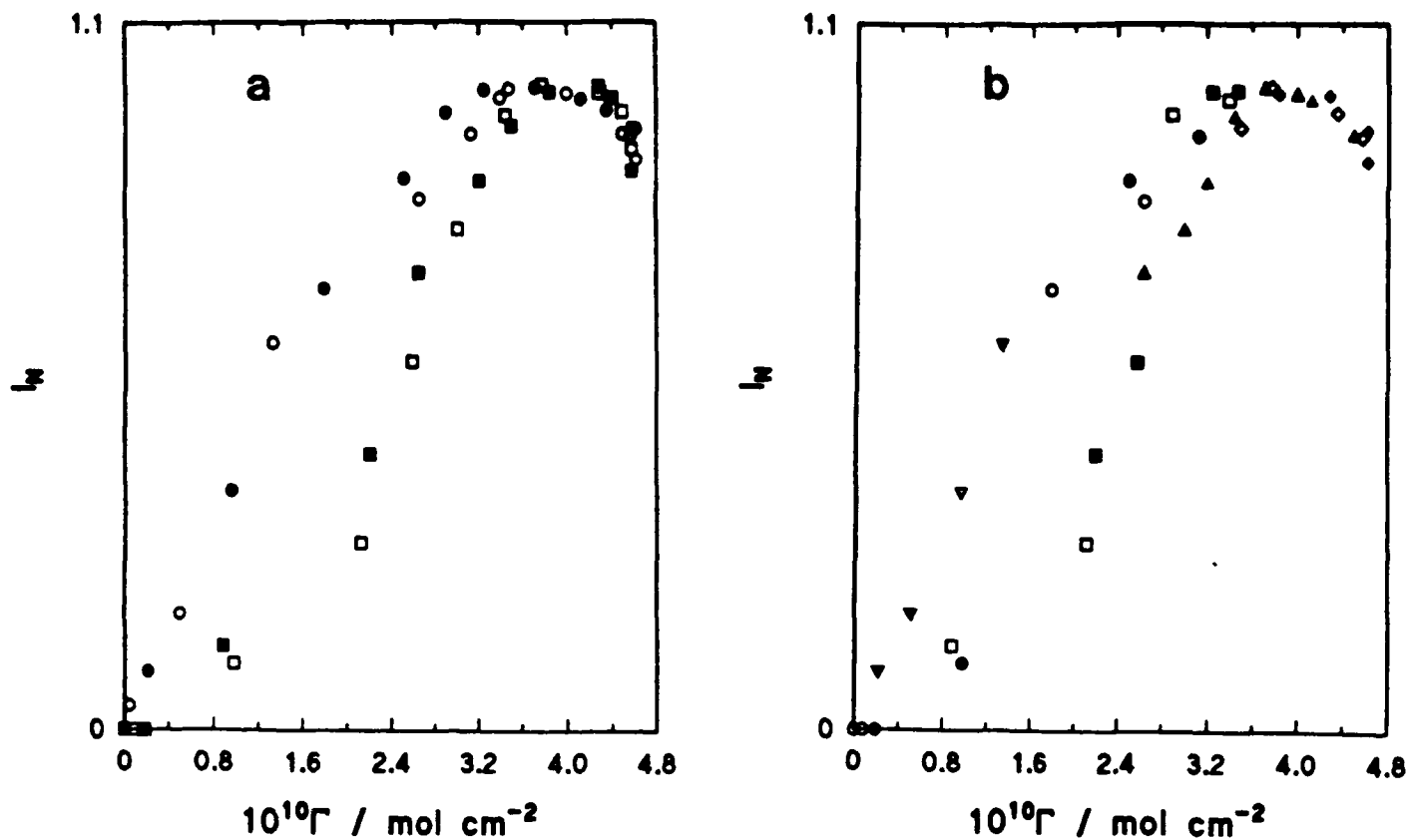


Figure 10.

Plots illustrating the relationship between  $I_N$  and  $\Gamma$  for: (a) superimposition of the data presented in Figure 7. Data for the following bulk pyridine concentrations are shown: (O)  $3 \times 10^{-3}$  M; (●)  $10^{-3}$  M; (□)  $10^{-4}$  M; (■)  $4 \times 10^{-5}$  M and (b) constant electrode potential. Data for the following electrode potentials are presented: (▼)  $-0.65$  V; (▽)  $-0.6$  V; (○)  $-0.55$  V; (●)  $-0.5$  V; (□)  $-0.45$  V; (■)  $-0.4$  V; (△)  $-0.35$  V; (▲)  $-0.3$  V; (◇)  $-0.25$  V; (◆)  $-0.2$  V.

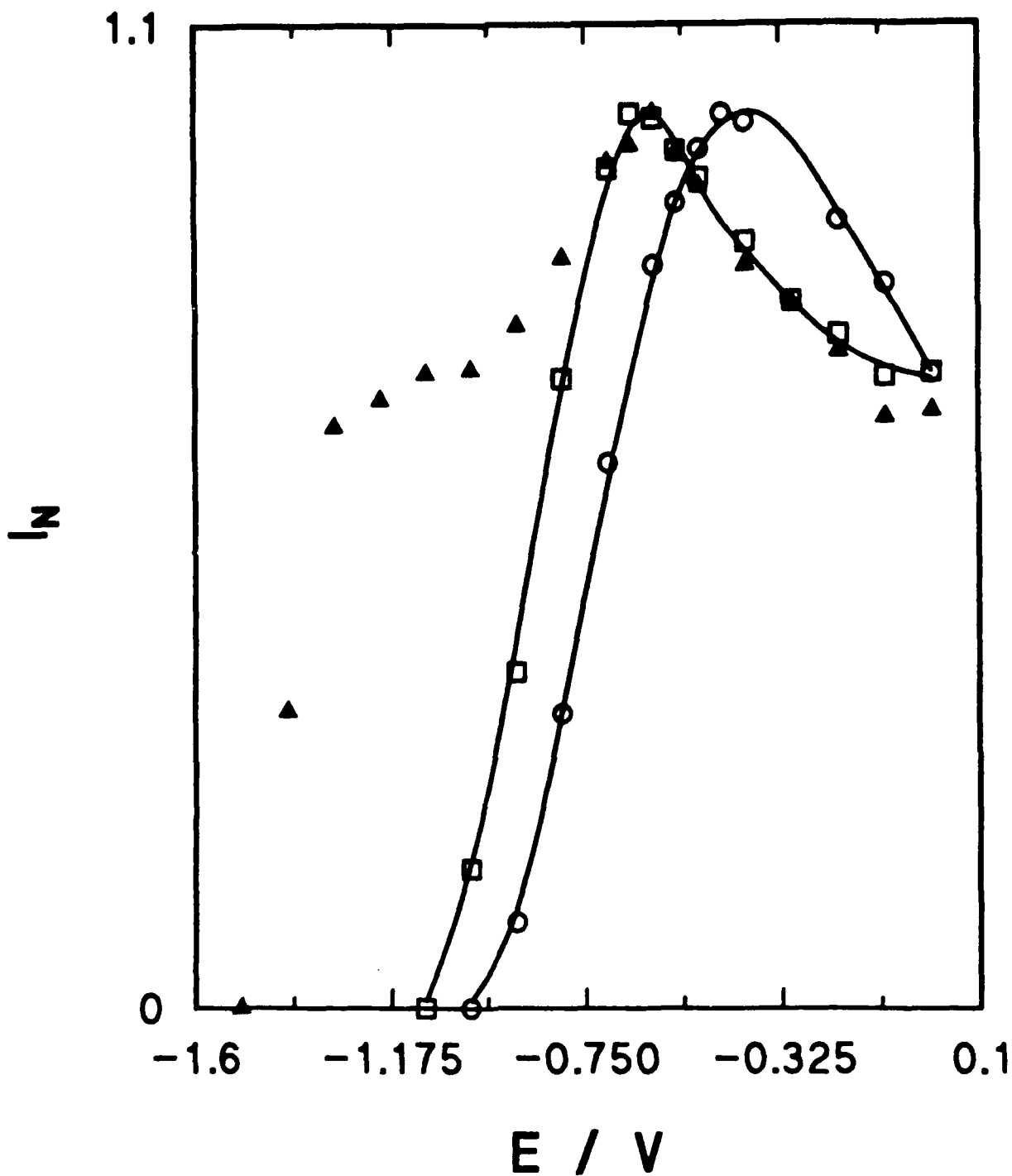


Figure 11.

$I_N$  versus  $E$  curves depicting the effect of surface roughness. (O) 1 ORC, 125 accumulations; (□) 7 ORC's, integration time - 3.0 s, 50 accumulations; (▲) 15 ORC's, 50 accumulations.

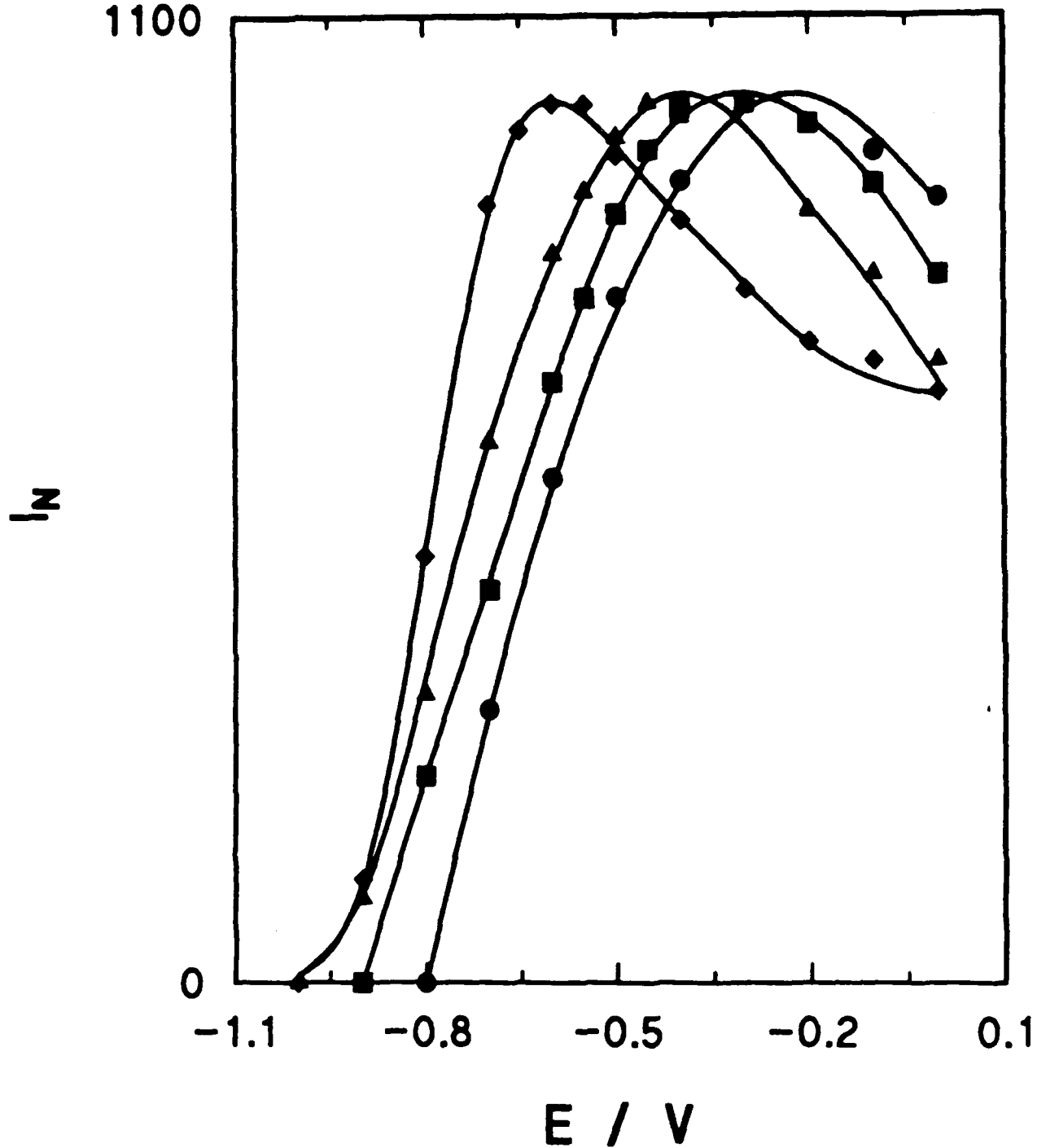


Figure 12.

Normalized band area versus electrode potential curves illustrating the effect of bulk pyridine concentration for a gold electrode subjected to 1 oxidation-reduction cycle.

(●)  $10^{-4}$  M, 3.0 s integration time; (■)  $5 \times 10^{-4}$  M; (▲)  $10^{-3}$  M; (◆)  $3 \times 10^{-3}$  M.  $5 \times 10^{-4}$  M - 150 accumulations, all other concentrations 125 accumulations.

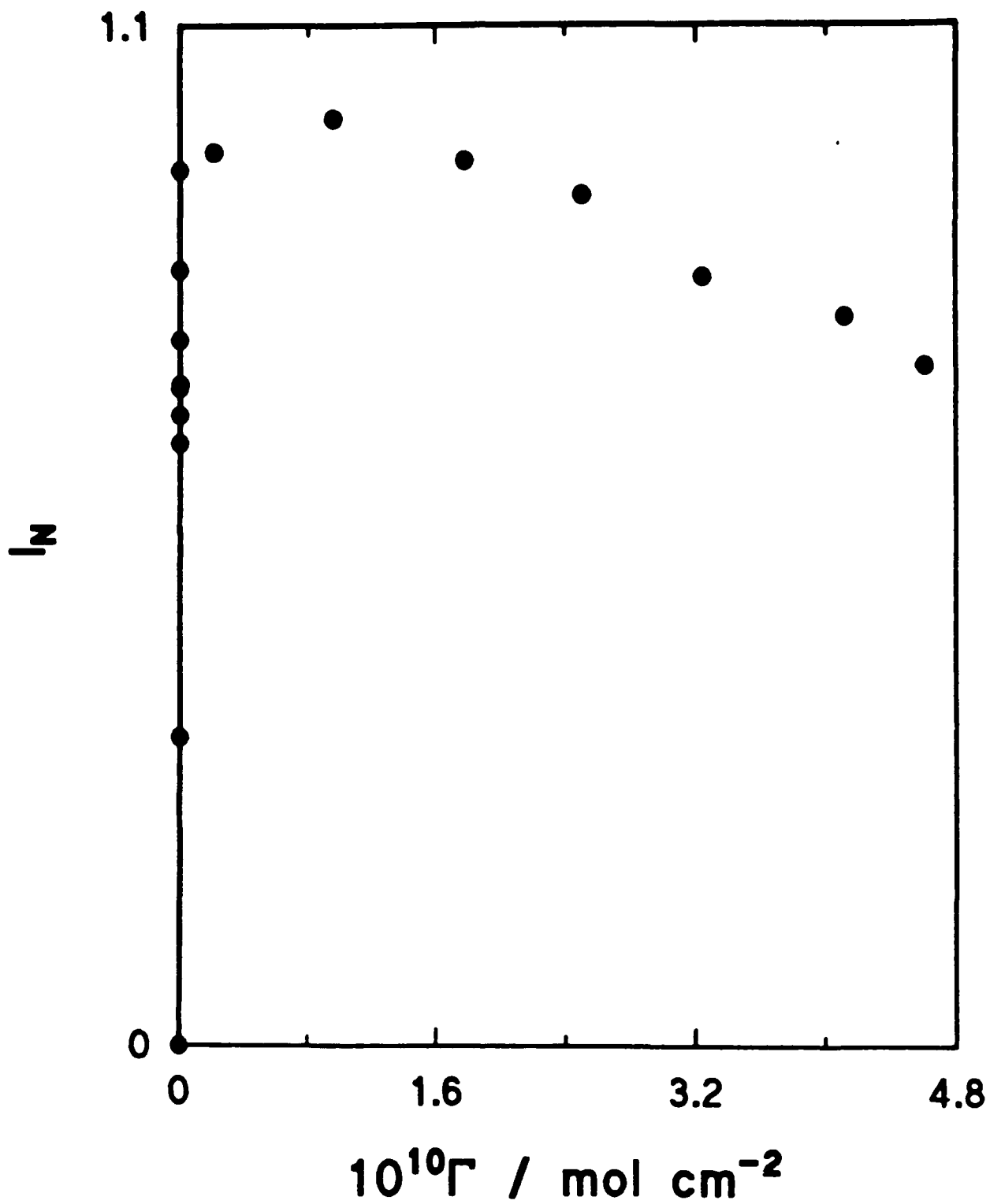


Figure 13.

Plot showing the relationship between  $I_N$  and  $\Gamma$  for a surface subjected to 15 oxidation-reduction cycles. The bulk pyridine concentration is  $10^3$  M.

TECHNICAL REPORT DISTRIBUTION LIST - GENERAL

Office of Naval Research (2)  
Chemistry Division, Code 1113  
800 North Quincy Street  
Arlington, Virginia 22217-5000

Commanding Officer (1)  
Naval Weapons Support Center  
Dr. Bernard E. Douda  
Crane, Indiana 47522-5050

Dr. Richard W. Drisko (1)  
Naval Civil Engineering  
Laboratory  
Code L52  
Port Hueneme, CA 93043

David Taylor Research Center (1)  
Dr. Eugene C. Fischer  
Annapolis, MD 21402-5067

Dr. James S. Murday (1)  
Chemistry Division, Code 6100  
Naval Research Laboratory  
Washington, D.C. 20375-5000

Defence Technical Information (2)  
Center  
Building 5  
Cameron Station  
Alexandria, VA  
U.S.A. 22314

Dr. Robert Green, Director (1)  
Chemistry Division, Code 385  
Naval Weapons Center  
China Lake, CA 93555-6001

Chief of Naval Research (1)  
Special Assistant for Marine  
Corps Matters  
Code 00MC  
800 North Quincy Street  
Arlington, VA 22217-5000

Dr. Bernadette Eichinger (1)  
Naval Ship Systems Engineering  
Station  
Code 053  
Philadelphia Naval Base  
Philadelphia, PA 19112

Dr. Sachio Yamamoto (1)  
Naval Ocean Systems Center  
Code 52  
San Diego, CA 92152-5000

Dr. Harold H. Singerman (1)  
David Taylor Research Center  
Code 283  
Annapolis, MD 21402-5067

ENCLOSURE(2)